ELSEVIER

Journal of Power Sources 109 (2002) 365–376

JOURNAL OF POWER SOURCES

www.elsevier.com/locate/jpowsour

Simulating process settings for unslaved SOFC response to increases in load demand

Comas Haynes*

Georgia Tech Center for Innovative Fuel Cell and Battery Technologies, Georgia Tech Research Institute, Atlanta, GA 30332-0853, USA

Received 18 December 2001; accepted 16 February 2002

Abstract

A common approach to reliable load-following is to ''slave'' fuel cell response to the reactants supply subsystem (e.g. fuel processor). A change-in-power demand may be time-sensitive, however, and slaving the fuel cell response to that of the slower balance-of-plant components may not be practical. A model has been constructed to simulate the *unrestrained* load-following characteristics of a commercial-grade fuel cell. Analyses have shown that initial conditions exist which facilitate timely responses to increases in load demand, among them lower fuel utilization, larger operating voltage and optimized cell potential reduction.

Keywords: Transient; Solid oxide; Unrestrained; Load-following

1. Introduction

Fuel cells, *themselves*, are excellent load-following devices. Part-load cell efficiencies are often greater than the full-load values, because a decrease in load may be accompanied by an increase in cell voltage. Additionally, fuel cells can respond sufficiently fast to changes in load due to the cells' rapid electrochemical response [1,2]. The primary issue in fuel cell *system* load-following is the relatively slow response of balance-of-plant components, particularly the reactants supply subsystem. As the primary example, fuel processors' load-following time constants are typically orders of magnitude greater than those of the corresponding fuel cells. This difference in response times may lead to undesirable constraints, such as delayed acceleration in fuel cell vehicles [3] and limitations in using fuel cells for load-varying distributed generation.

Fuel cell system load-following is facilitated, however, when the fuel cells are not *slaved* (i.e. coupled) to longer fuel processor time constants. The fuel cell stack would thus be allowed to rapidly load-follow, while the fuel processor is in the initial phases of its transient response. Kreutz and Ogden [3] and Liese et al. [4] also acknowledge the enhancement to system response when the decoupled cell stack is allowed to freely respond to load excursions. These authors, however, cautioned that such load-following has major limitations; thus, accurate dynamic modeling is critical to employing such a control scheme safely. The objective was thus to model and identify operating conditions trends wherein cell stacks could reliably accommodate increases in load without being restrained by fuel processing delays.

Tubular solid oxide fuel cell (TSOFC) technology was simulated in this study. This technology has distinctive features. Solid oxide fuel cells (SOFCs) are solid state, ceramic cells that conventionally operate within a temperature range of 800–1000 °C. Note that ''low'' temperature SOFCs operate in a temperature range of 550–800 °C. Their high operating temperatures preclude the need for expensive catalysts on the electrodes. Carbon monoxide, which is a by-product gas present in hydrogen-rich reformate (synthesis gas), is not harmful to the cells but can be used as a fuel. The cells reject high quality heat that can be used for a number of needs (i.e. fuel processing, thermal energy for bottoming heat engines, etc.). Additionally, the solid electrolyte precludes management issues often encountered with liquids (e.g. volatility, corrosion, composition change). Finally, the all solid-state cell allows for novel geometries. Amongst the prevalent designs is the tubular geometry shown in Fig. 1.

Fig. 1 illustrates the design of the SiemensWestinghouse TSOFC technology. The inner layer is a modified lanthanum manganite cathode (air electrode). Previously there was a support tube that air had to diffuse through, but the current generation of TSOFC technology is air electrode-supported. The electrolyte is made of yttria-stabilized zirconia. The anode, or fuel electrode, is made of a nickel–zirconia cermet. Current is extracted from an interconnect material of doped lanthanum chromite. Finally, nickel felt contact padding (not

* Tel.: +1-770-528-7578; fax: +1-770-528-7028/7083.
E-mail address: comas.haynes@gtri.gatech.edu (C. Haynes).

0378-7753/02/$ – see front matter
PII: S0378-7753(02)00088-5

Nomenclature

A	surface area (m^2)
Bi	Biot number
c_p	specific heat at constant pressure (J/kg K)
$\dot{C}$	heat capacity rate (W/K)
D	diameter (m)
E	Nernst potential (J/C)
$\dot{E}$	thermal energy rate (J/s)
h	convective heat transfer coefficient (W/m^2 K)
i	current (C/s)
k	thermal conductivity (W/m s)
L	length (m)
$\dot{m}_j$	mass flow rate of j (kg/s)
$\dot{n}_i$	molar flow rate of constituent i (mol/s)
Nu	Nusselt number
P	perimeter (m)
P	power (W)
$\dot{Q}$	heat (J/s)
R	resistance (Ω)
t	time (s)
T	absolute temperature (K)
T_s	time to steady-state (s)
v	velocity (m/s)
V	voltage (J/C)
x	distance (m)

Greek letters

Δ	change in quantity
ε	emissivity
η	fluid properties
θ	dimensionless temperature coefficient
σ	Stefan–Boltzmann constant (5.67×10^{-8} W/K^4)

shown) serves as a means of connecting individual cells to form arrays (stacks). Primarily due to a longer current path length, TSOFCs' area-specific internal resistances are larger than planar SOFC geometries; thus, their power densities are typically smaller. Despite the performance penalty that results from cell geometry, there are benefits to product integrity. As an example, the cells have a seal-less feature that mitigates a number of degradation effects associated with high temperature SOFCs; additionally, the TSOFC technology has established availability records within the fuel cells industry. The present work is quantitatively specific to TSOFC technology; yet, the qualitative findings are applicable to various fuel cell designs.

As alluded to previously, the proposed tactic of decoupled cell stack load-following can be detrimental if the process dynamics are poorly understood and load-following is not done judiciously. Padulles et al. [5] considered an integrated SOFC system operating dynamically, and they highlighted hazardous scenarios: underutilized fuel (small fuel utilization) causing cell voltage to rise at an unacceptable rate; overused fuel (large fuel utilization) causing the cells to

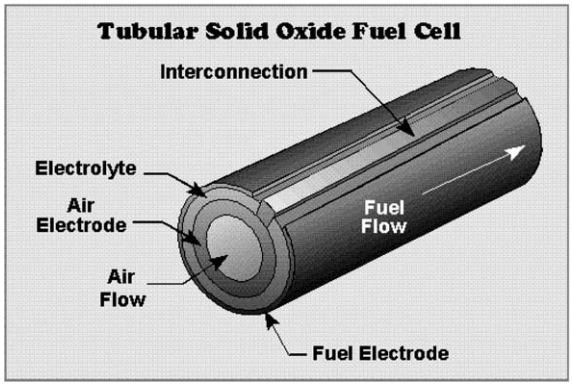

Fig. 1. Isometric view of SiemensWestinghouse TSOFC.

suffer from fuel starvation; undervoltage (output voltage smaller than an established minimum) causing a loss of synchronism within the power conditioning subsystem. Note that Padulles et al. presented an analysis of SOFC transients with a large emphasis on power conditioning, while the current paper focuses on power generation. Additionally, as will be explained, an intended increase in power generation may actually result in a decrease if *unslaved* load-following is done erroneously. Unintended electrical response is not the only cause for concern; cell temperature rise may be detrimental. As an example, TSOFCs nominally operate at 1000 °C to reduce ohmic losses. Minh and Takahashi [6] report deleterious chemical reactions between cathode and electrolyte near 1100 °C. These two temperatures are close enough that the thermal response to increased load could degrade the cell. Electrical and thermal transient effects have thus been simulated to predict the (initial) operating conditions and subsequent time frames within which hikes in load demand can safely be accommodated without constraining the cell stack's response.

2. Model description

2.1. Assumptions/simplifications

2.1.1. Potentiostatic control

A potentiostatic control strategy is predicated, wherein current and power generation are changed through prescribed voltage drops. This scenario facilitated the extension of an experimentally validated TSOFC electrochemical model [7] to analyze transient events, since the referenced model was based upon operating voltage being a decision variable. The appropriateness of the results are not constrained to potentiostatic controls schemes, however, since the research findings were primarily functions of process *end states* (i.e. initial conditions and final cell voltage/current density).

The model numerically simulates electrochemistry along the cell. This is inherently more accurate than the work of Costamagna et al. [8], since these authors analyzed a

TSOFC/micro-gas turbine hybrid system without incorporating specific TSOFC geometrical details (for generality). Additionally, they utilized a macroscopic, finite control volume approach to facilitate computations.

2.1.2. Multiple time scales of transport phenomena

Transient phenomena occur over three time scales. Electrochemical devices have nearly instantaneous load response in comparison to thermal-hydraulic phenomena [3]; thus, electrochemical transient response was assumed sufficiently fast to presume quasi-steady electrochemistry (i.e. steady-state electrochemistry on an instant-by-instant basis). Note that the neglect of *electrochemical* transient response does not preclude analyzing *electrical* transient effects. Unsteady electricity generation results from changes in reactant presence along the cell. Fluid flow is thus a rate determining transport phenomenon. Finally, in comparison to the *electrochemical* and *electrical* time scales, *thermal* transients involve significantly larger time constants. As the reader shall see, results verified that cell temperature rise could be simulated as a phenomenon that occurs after electrical transients end. The verification is discussed in Section 2.3.

2.1.3. Invariant fuel and oxidant supply

The model assumes that both the supply and inlet properties of reactants remain invariant throughout the electrical transient (i.e. from initial to final electrical steady-state). This highlights the orders of magnitude difference between the response time constants of the cell stack and reactants supply subsystem. Achenbach also incorporated an invariant reactants supply scenario within his model of SOFC transients [9]. His simulations, however, prefaced that before the cell stack responded to changes in load, the reactants streams had already been adjusted. This approach thus continued to constrain the overall system response to that of the slowest component(s).

2.1.4. Thermal lumped capacitance

Fig. 2 shows thermal transport *within* a TSOFC. Air is supplied to the cell by means of an alumina oxide supply pipe. Upon exiting the air supply pipe (into the closed end of the cell), the air reverses direction and serves as the oxidant stream. Exterior to the cell, fuel flows in the same direction as the oxidant stream. Electrochemical phenomena between electrode surfaces generate thermal energy, and heat transfer occurs by means of radiation and convection. Further details are given in Haynes and Wepfer [10].

A lumped capacitance methodology was used, in which structural temperatures (i.e. those of the air supply pipe and fuel cell) were assumed uniform and thus sole functions of time. Consider the Biot number of the cell:

$$\mathrm{Bi}_{\mathrm{cell}} = \frac{hL_{\mathrm{char,\,cell}}}{k_{\mathrm{solid}}} \tag{1}$$

The Biot number is a dimensionless term used to investigate transient heat transfer. It represents the ratio of conductive resistance to convective resistance; an electrochemical analogy to the Biot number is the Wagner number, which represents the ratio of charge transfer resistance to ohmic resistance. Haynes and Wepfer [10] explained the dominance of radial heat transfer in TSOFCs. The cells' characteristic length (in the Bi formulation) is then on the order of their thickness; their relatively small thickness (on the order of millimeters in comparison to an axial length on the order of meters) leads to low Biot numbers. Specifically, the Biot number of the fuel cell

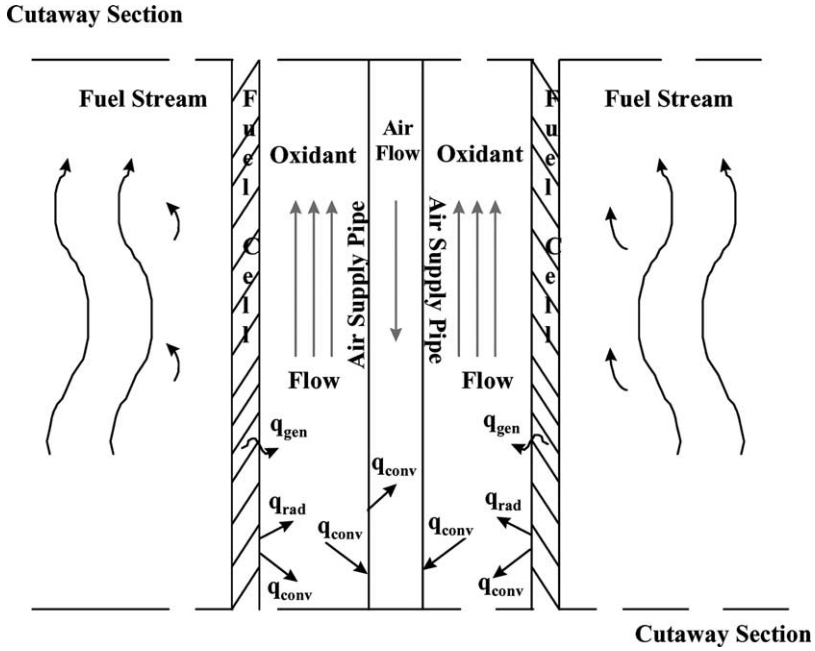

Fig. 2. Thermal transport phenomena within the cell interior.

was consistently calculated at less than one-tenth, meaning structural temperature gradients are small in comparison to temperature differences across the thermal boundary layer. Lumped capacitance is then an appropriate approach to cell thermal analysis [11]. The air supply pipe is an ancillary structure within each cell that is also modeled through lumped capacitance due to its small characteristic (i.e. radial) length [10]. Amphlett et al. used lumped capacitance in their analysis of fuel cell transient behavior [12], as did Liese et al. in their analysis of SOFC transient behavior [4].

2.1.5. Quasi-steady heat transfer/air is the dominant heat sink

Quasi-steady convective heat transfer is assumed, with air modeled as the dominant heat sink. Again the proposed controls tactic incorporates decoupled cell response to increased load demand. A hazard of such load-following is the excessive thermal energy generation that results; more current is generated but with an invariant heat sink (i.e. oxidant flow rate). The quasi-steady model is commonly used in transient convection analysis [13]. Air was the dominant heat sink, since it usually has a much larger heat capacity rate than the fuel stream. Additionally, external fuel processing was presumed; thus, the reformate inlet temperature would be much closer to the cell's temperature than that of the oxidant stream. Finally, an empirical envelope loss coefficient was used, as in the work of Amphlett et al. [12].

The National Fuel Cell Research Center (NFCRC), in conjunction with the National Energy Technology Laboratory (NETL) also performed transient analyses of SOFCs [4,14], and their models incorporated a number of the above assumptions. Their controls approach, however, was based upon the standard allowance for fuel processing transients to precede cell stack load-following. Finally, while the emphasis of their transient studies was load *decrease*, the present paper focuses on load *increase.*

2.2. Electrical transient response model

Although *electrochemical* transient responses are fast in comparison to thermal-hydraulic transients, finite *electrical* transient effects still arise due to changes in constituent concentrations.

Fig. 3 is a schematic of the hydrogen concentration profile along the fuel cell. The solid curve concentration profile corresponds to the cell's initial steady-state. At $t = 0+$, the operating voltage decreases to accommodate an increase in

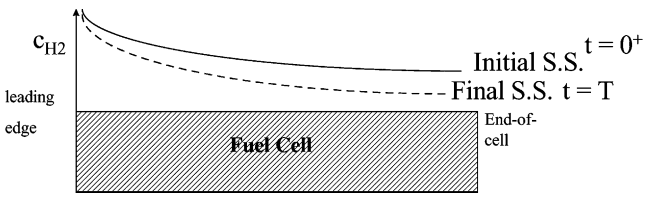

Fig. 3. Illustration of fuel stream transient dynamics.

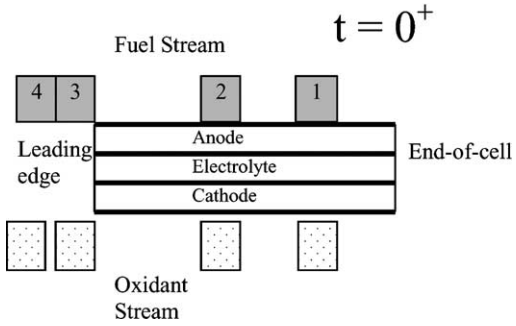

Fig. 4. Individual fuel element locations at the time of the load hike (Lagrangian approach).

load demand. The reactants supply, however, is predicated on the prescribed fuel utilization and initial current. In accordance with Faraday's Law, there is a decline in reactant concentrations when the load increases. This decrease continues until a new electrical steady-state is reached (at $t = T_s$). Transient analyses are facilitated by focusing attention on individual fluid elements as they travel along the cell; this method is called a Lagrangian approach.

Fig. 4 illustrates the Lagrangian approach. During the cells' transient response to load increase, each fuel element approaches the cell with the same inlet characteristics, as explained within assumption no. 3. The exit properties of each fluid element, however, depend upon its location at the time of the load hike, $t = 0+$. Element 2 of Fig. 4, for example, will have greater reactant depletion than element 1. This is because element 2 has longer exposure to electroactive area at the lower operating voltage. The *electrical* transient episode ensues until each fluid element approaching the cell again experiences an identical change in constituents. This occurs when element 3 reaches the end of the cell (note element 3 is at the beginning of the cell when the cell potential decreases). After element 3, every subsequent fluid element (e.g. element 4) enters at the new operating voltage; these elements then experience the same reaction phenomena. The time of the electrical episode is thus nearly the length of the cell divided by the fuel velocity. Depending on fuel flow rate, the time frame of the electrical transients is a fraction of a second. Note that fuel processors have response times on the orders of seconds (e.g. partial oxidation units) and minutes (e.g. steam reformers).

By inspection of Figs. 4–6, the reader sees that less emphasis is placed upon oxidant stream property variation (i.e. the oxidant stream elements are not distinguished from each other through numbers). Air stoichiometric numbers, or inverse equivalence ratios, are typically >1 (e.g. ranging from 4 to 6) for conventional thermal management; this is especially the case when there is no internal reformation to absorb thermal energy from the cells. The oxygen mole fraction is thus more stable along the cathode. As an example, consider the operational extreme of a relatively low air stoichiometric number of 3 and an unrealistically high fuel utilization of unity. The inlet oxygen percentage is approximately 21%; the

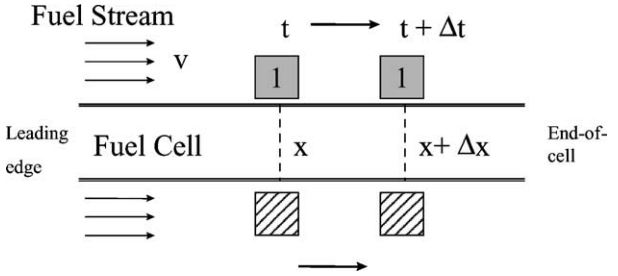

Fig. 5. Correlation between temporal and spatial discretizations.

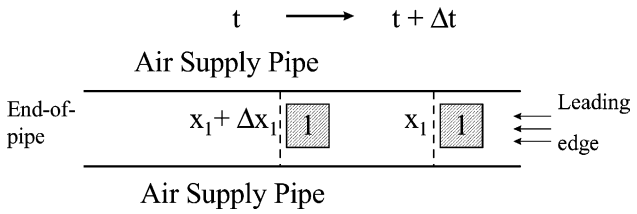

Fig. 6. Lagrangian methodology for transient temperature profiles within the air supply pipe.

exit mole fraction would be nearly 15%. Simulations showed a current/power variation of only a few percent caused by such a difference in oxygen mole fraction.

Additionally, a previous publication [10] explained how the TSOFC's slender geometry, its high operating temperature and the large number of transfer units (NTU) within the air supply pipe cause the oxidant stream to essentially be in thermal equilibrium with the cell throughout the annular region. The small variation of oxidant mole fraction and temperature along the cathode resulted in the primary focus being placed upon fuel stream dynamics (for analysis of electrical transients).

The fluid elements involved in the transient episodes were computationally "tracked." This was done through two-dimensional arrays containing field variable information (i.e. axial position and time). The Lagrangian basis is that a fluid element occupies a certain location at a given time.

$$\eta_{\text{element, fluid}} = \eta(x,\, t) \tag{2}$$

The symbol η represents the properties of the fluid element in question (e.g. constituent partial pressures). The electrical power produced along the cell depends upon these properties. In accord with the Lagrangian methodology, the temporal discretization is compliant with the flows' velocity and the axial discretization of the cell (i.e. slice lengths).

$$\Delta t = \frac{\Delta x}{v} \tag{3}$$

The following figure illustrates the principle.

Considering Eqs. (2)–(3), the following relation results.

$$\eta_{\text{fluid, element}}(t + \Delta t) = \eta(x + \Delta x,\, t + \Delta t) \tag{4}$$

The quasi-steady-state electrochemistry assumption means that electrochemical phenomena occur as if at steady-state, at the given instant. A proven steady-state electrochemical model [7] was thus utilized to predict current, power and heat generation. This was done by applying a relation equivalent to the Reynolds Transport Theorem [15].

$$\dot{n}_{\text{j, intermed}}(x + \Delta x,\, t + \Delta t) = \dot{n}_{\text{j, entering, slice}}(x,\, t) + \Delta\dot{n}_{\text{j}}(x,\, t) \tag{5}$$

The "j" subscript represents hydrogen, oxygen and steam, and Eq. (5) accounts for the temporal change in constituents due to electrochemical oxidations.

$$\dot{n}_{\text{k}}(x + \Delta x,\, t + \Delta t) = \dot{n}_{\text{k, intermed}}(x + \Delta x,\, t + \Delta t) + \dot{n}_{\text{k, shift, change}}(\vec{x},\, t) \tag{6}$$

The "k" subscript represents hydrogen, steam, carbon monoxide and carbon dioxide. Eq. (6) accounts for the temporal change in constituents due to the shift reaction, which was modeled through equilibrium chemistry due to the hot fuel stream and nickel catalyst within the anode. These temporal expressions of mass conservation enabled the transient electrochemical model to "march out" in time. Thermal transient effects were also considered.

2.3. Thermal transient model

2.3.1. Cell thermal response

Thermal transport phenomena were illustrated in Fig. 2. The primary step in analyzing the thermal response of the fuel cell is to establish its time dependent thermal energy balance.

$$\dot{E}_{\text{stored, cell}} = \dot{E}_{\text{gen, cell}} - \dot{E}_{\text{out, cell}} \tag{7a}$$

$$\dot{E}_{\text{stored, cell}} = C_{\text{cell}} \frac{\mathrm{d}T_{\text{cell}}}{\mathrm{d}t} \tag{7b}$$

$$\dot{E}_{\text{out, cell}} = \dot{Q}_{\text{rad}} + \dot{Q}_{\text{TFD}} + \dot{Q}_{\text{cell, convect, ann}} \tag{7c}$$

$$\dot{Q}_{\text{rad}} = \varepsilon_{\text{ASP}}\sigma A_{\text{ASP}}(T_{\text{cell}}(t)^4 - T_{\text{ASP}}(t)^4) \tag{7d}$$

Eq. (7a) is the conservation of thermal energy applied to an unsteady (transient) system. The electrochemical model predicts the generation term. The volume of the TSOFC and its reported volumetric heat capacity determine its overall heat capacitance. The first term on the right hand side of Eq. (7c) is the radiation from the cell to the air supply pipe. The latter terms in this equation quantify heat convection from the cell to the oxidant in the annulus. The quasi-steady-state heat transfer assumption is used to calculate these terms.

$$\dot{Q}_{\text{TFD}} = \dot{m}_{\text{air}}\bar{c}_p(T_{\text{air, bulk, terminal}}(t) - T_{\text{air, exit, ASP}}(t)) \tag{8a}$$

$$T_{\text{air, bulk, terminal}}(t) = \theta_{\text{Bi}}^{(1)} T_{\text{ASP}}(t) + \theta_{\text{Bi}}^{(1)} T_{\text{cell}}(t) \tag{8b}$$

$$\dot{Q}_{\text{cell, convect, ann}} = \text{Nu}_{00}^{(1)} \frac{k_{\text{air}}((T_{\text{cell}}(t) + T_{\text{air, bulk, terminal}}(t))/2)}{D_h} \times A_{\text{ann, cell}}(T_{\text{FC}}(t) - T_{\text{air, bulk, terminal}}(t)) \tag{9}$$

Eqs. (8) and (9) are equations for the convection within, and beyond, the annulus entrance. These equations comprise

the quasi-steady convection model alluded to in assumption no. 5. As in the SOFC transient analyses of Liese et al. [4], fluid flow is presumed fully developed. Note the change in fuel cell temperature is coupled to the air supply pipe temperature both explicitly through radiation and implicitly through convection (the air entering the annulus is first preheated in the pipe). Resolving the temporal profile of the fuel cell's temperature then requires calculating the temperature response of the air supply pipe as well.

2.3.2. Supply pipe temperature response

An energy balance is again developed.

$$\dot{E}_{\text{stored, ASP}} = \dot{E}_{\text{in, ASP}} - \dot{E}_{\text{out, ASP}} \tag{10a}$$

$$\dot{E}_{\text{stored, ASP}} = C_{\text{ASP}} \frac{\mathrm{d}T_{\text{ASP}}}{\mathrm{d}t} \tag{10b}$$

$$\dot{E}_{\text{in, ASP}} = \dot{Q}_{\text{rad}} + \dot{Q}_{\text{cell, convect, ann}} \tag{10c}$$

$$\dot{E}_{\text{out, ASP}} = \dot{Q}_{\text{ASP}\rightarrow\text{air, inside}} \tag{10d}$$

The heat capacitance term of Eq. (10b) is based on supply pipe volume and volumetric heat capacity data for alumina oxide [16]. Eq. (10c) results from two considerations. The net heat radiated from the cell has to be absorbed by the supply pipe, since air is a non-participating medium. Additionally, the attainment of a terminal bulk temperature in the annulus entrance precludes heat gain by the fully developed flow [10]. The convective heat from the cell to the oxidant stream thus continues convecting to the air supply pipe. Eq. (10d) is next discussed.

Unlike the annular region, the fluid temperature inside the air supply pipe has a profile that is non-uniform and initially exponential. In compliance with this axial variation of bulk temperature, convection within the air supply pipe is modeled as a surface integral.

$$\dot{Q}_{\text{ASP}\rightarrow\text{air, inside}} = \int_{\text{length, ASP}} [h(x)(T_{\text{ASP}}(t) - T_{\text{bulk}}(x, t))] P \,\mathrm{d}x \tag{11}$$

The integrand of Eq. (11) is the product of convective heat flux and the supply pipe's inner perimeter. Note the time dependence of the convective heat transfer coefficient is negated. This simplification is in accord with the quasi-steady-state heat transfer methodology used by Amphlett et al. [12] in their thermal response analyses of fuel cells. The reader is reminded that the fluid streams supply remains invariant with time. The flows are hence presumed steady, and there is no change in flow regime (i.e. laminar-to-turbulent or vice versa). The spatial dependence of the convective heat transfer coefficient is reported in another reference [17].

2.3.3. Temperature profiles of air supply as a function of time

The change in annulus terminal bulk temperature is compliant with the changes in fuel cell and supply pipe temperatures, through Eq. (8b). The change in temperatures of the air "elements" within the supply pipe may be calculated in Lagrangian fashion.

Presuming a sufficiently small time increment:

$$\dot{C}_{\text{flow}}[T_{\text{bulk}}(x_1 + \Delta x_1, t + \Delta t) - T_{\text{bulk}}(x_1, t)] = h(x_1) P \Delta x_1 (T_{\text{ASP}}(t) - T_{\text{bulk}}(x_1, t)) \tag{12}$$

Algorithm to calculate changes in temperatures.

2.3.4. Algorithm

Following the precedent set by Amphlett et al. [12], the Euler (numerical) method was utilized. It was applied to the structural temperatures discussed above: cell temperature and supply pipe temperature.

$$T_{\text{j}}(t + \Delta t) = T_{\text{j}}(t) + \left(\frac{\mathrm{d}T_{\text{j}}}{\mathrm{d}t}\right)_t \Delta t \tag{13}$$

The model's time steps were relatively small (on the order of milliseconds) when compared to the thermal responses of the cells (on the order of minutes). Again the diminutive time steps were in (Lagrangian) compliance with reactant stream velocities and slice lengths. The simplicity of the Euler method eased computational burden, and negative attributes of the Euler method (less accuracy, tendency for instability) were mitigated through small time steps [18]. The following algorithm was used to predict thermal response.

1. Establish the *initial* steady-state temperatures based upon the author's previously published model [10].
2. Resolve the changes in electricity.
3. Establish the *new* steady-state thermal energy production due to fuel cell operation (i.e. the new heat generation after electrical changes cease).
4. To calculate the changes in pertinent temperatures following steps are required.
   (i) Calculate the heat transfers (Eqs. (7d)–(9), (11)).
   (ii) Calculate the changes in bulk temperatures within the supply pipe (Eq. (12)).
   (iii) Calculate the changes in fuel cell and supply pipe temperatures (Eqs. (7a–c), (10) and (13)).
   (iv) If the new cell temperature reaches or surpasses 1050 °C (halfway point to the degradation temperature) or does not change from the previous value by more than 0.5%, stop the algorithm.
   (v) Calculate the change in annulus, terminal bulk temperature (Eq. (8b)).
   (vi) Return to (i).

2.4. Case study results

A representative case is presented wherein electrical and thermal transient results are reported and discussed. Table 1 contains the initial (baseline) conditions. A number of the settings are a compilation of test conditions reported by

Table 1
Baseline conditions used in the transient case study

Pressure (atm)	3
Stoichiometric number	3
Fuel utilization (%)	85
Operating voltage (V)	0.6
Inlet methane mole fraction	5E−5
Inlet hydrogen mole fraction	0.67
Inlet carbon monoxide mole fraction	0.22
Inlet steam mole fraction	0.11
Inlet carbon dioxide mole fraction	1E−4
Power conditioning efficiency (%)	95

SiemensWestinghouse and the Department of Energy [19,20].

A 0.1 V decrease (to 0.5 V) occurs at "$t = 0+$". Besides fuel utilization (discussed shortly), all other baseline conditions remain fixed. The changes in electricity are first discussed.

2.4.1. Electrical response

The following figures illustrate the electrical response resulting from the attempted load-following.

The voltage drop *event* corresponds to the spikes shown in Fig. 7. The percentage increase in power is not as great as that of the increase in current. Although current increases, it was simultaneous with a voltage decrease. The result is a dampened rise in power. Subsequent to these initial spikes, current and power decrease. Over half of the gain in current is lost, and the final power output is *less* than its initial value. These undesired effects stem from the decreased reactant concentrations along the cell. An explanation follows.

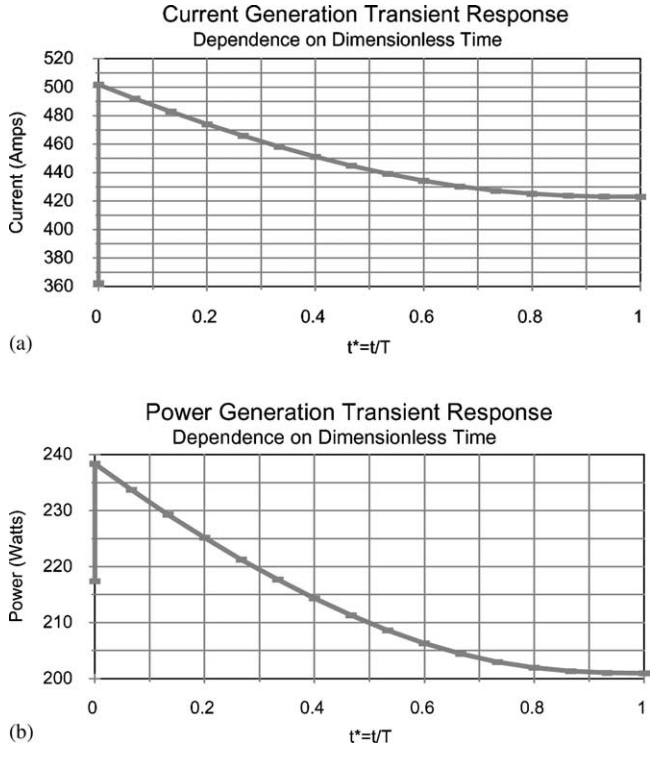

Fig. 7. (a) Variation of current with dimensionless time; (b) variation of power with dimensionless time.

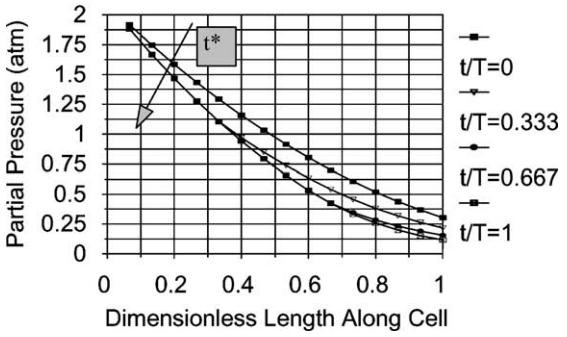

Fig. 8. Axial profiles of hydrogen partial pressure as functions of time.

Fig. 8 shows the decrease in hydrogen partial pressures throughout the time period (T_s) of the electrical response. The initial increase in current, shown in Fig. 7(a), consumes an excess of the fuel stream's hydrogen content. An effect-and-countereffect then develops between current generation and fuel utilization.

Fig. 9 illustrates the rise in fuel utilization during the transient episode. The additional current and invariant fuel supply results in an *increase* in fuel utilization. The increase in fuel utilization, in turn, promotes current *reduction*, because reactant depletion issues (e.g. concentration polarization, smaller Nernst potentials) become more pronounced. The effects of each upon the other cause current and fuel utilization to change accordingly until current electrochemically "matches" the original reactants supply rate and the new operating voltage. Fuel utilization then reaches a terminal value, and changes in electricity cease; this is neglecting second order effects of diminutive temperature rise during the timescale of *electrical* transients.

The current reduction here causes the power to fall below its initial value, because the decrease in operating voltage supersedes the *net* increase in current. An attempt at rapidly increasing the power output of a cell stack, through

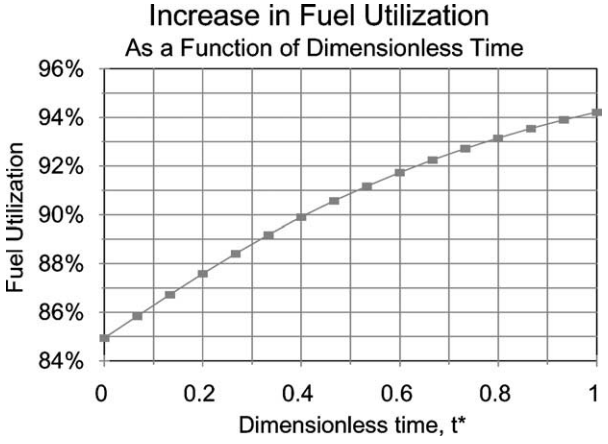

Fig. 9. Increase in fuel utilization during electrical transient episode.

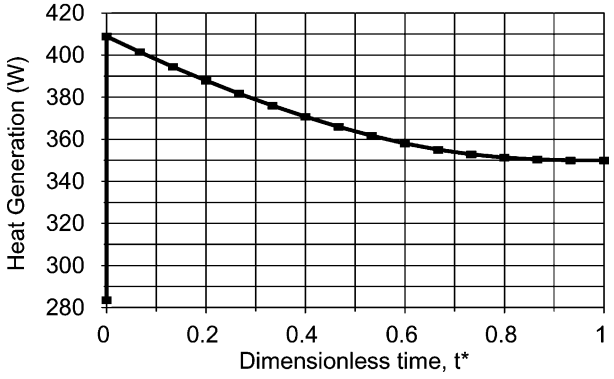

Fig. 10. Heat generation as a function of time.

independent load response, may actually lead to a rapid decrease in power generation; additionally, too large an increase in current may lead to dangerously high fuel utilizations (e.g. >95%). As will be shown, however, appropriate process settings facilitate using this rapid response controls scheme.

2.4.2. Thermal response

Fig. 10 contains the profile of heat generation as a function of dimensionless time. Heat generation is dependent upon current generation and thus has a similar time profile. The reader is reminded that electrical transients are typically fractions of a second. The change in heat generation is then *orders of magnitude* faster than the other thermal responses.

Fig. 11 contains the transient temperature profiles of both the fuel cell and the air supply pipe. The pipe's thermal diffusivity is large enough for its change in temperature to quickly follow that of the fuel cell. For the given case, the fuel cell would reach the maximum allowable cell temperature (in this case taken to be 1050 °C or 1323 K) 12.5 min after the voltage drop. This has various implications.

First, the drastically different time constants between transient heat generation and the structural temperature changes justify the approximation of heat generation as a constant quantity throughout the thermal transient response of the cell. The safety analysis does not allow for cell temperature to rise more than 50 °C; hence, material resistivities are assumed to be nearly constant. Secondly, the balance-of-plant would have minutes within which to increase the reactant flows (particularly air) before the cell is thermally endangered. Numerous reactants supply subsystems can accommodate this; however, the greater the balance-of-plant inertia (e.g. larger power plant applications), the greater the concern involved. Finally, considering the relatively instantaneous change in current and power generation (in comparison to cell thermal response), the electrical and thermal response models may be decoupled from one another (i.e. confirmation of assumption no. 2).

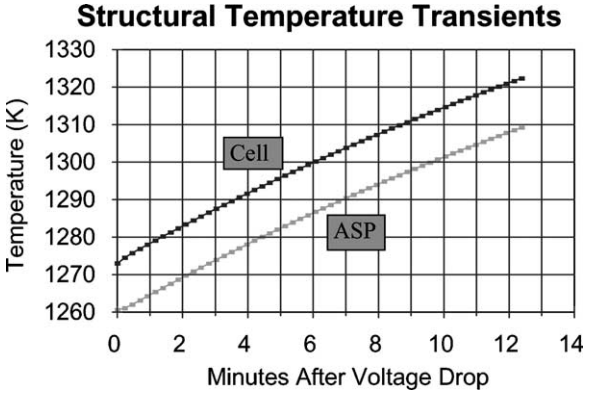

Fig. 11. Variation of structural temperatures as functions of time.

3. Process settings for effective load-following

The previous case study indicated the undesirable effects that may occur when attempting to raise cell power through unrestrained cell response. Despite these concerns, fuel cells must be able to effectively load-follow if they are to gain a niche in mainstream power generation. This is especially important when considering their expected mobile and decentralized applications. Fortunately, there are process settings that can help alleviate the issues of unslaved cell stack load-following.

3.1. Lower initial fuel utilizations

Lowering initial fuel utilization facilitates rapid increases in power generation. The surface graphs of Fig. 12 correspond to the baseline initial conditions within Table 1, with two modifications. Initial fuel utilization and operating voltage were parametrically varied. For uniformity of approach at the different settings (in particular initial operating voltages), each transient simulation involved a ten percent voltage drop.

It has been shown that an initial increase (i.e. spike) in current is followed by a decrease in current due to growing fuel utilizations (i.e. the fuel streams become depleted). The percentage current decrease is dependent upon the range of fuel utilizations involved. Consider the initial operating conditions given in Table 1, except initial fuel utilizations are 70 and 75%. In compliance with an increased load demand, operating voltage decreases 10%. An initial fuel utilization of 70% would rise to 78.8%. Current would spike from 430 to 511 A, and subsequently lower to 485 A. This is a 5.1% dip (i.e. decrease from peak value). If instead the initial fuel utilization is 75%, fuel utilization would rise to 83.7%. Current would spike from 416 to 496 A, and reach a terminal value of 464 A. This is a 6.5% dip. The current transients are illustrated in Figs. 13 and 14. Despite the near-equivalent gains in fuel utilization percentage points, the (initial condition) case of 70% results in significantly smaller current dip (i.e. power loss).

Lower fuel utilizations result in higher concentrations of unused reactants along the cell. There is thus a ''virtual fuel

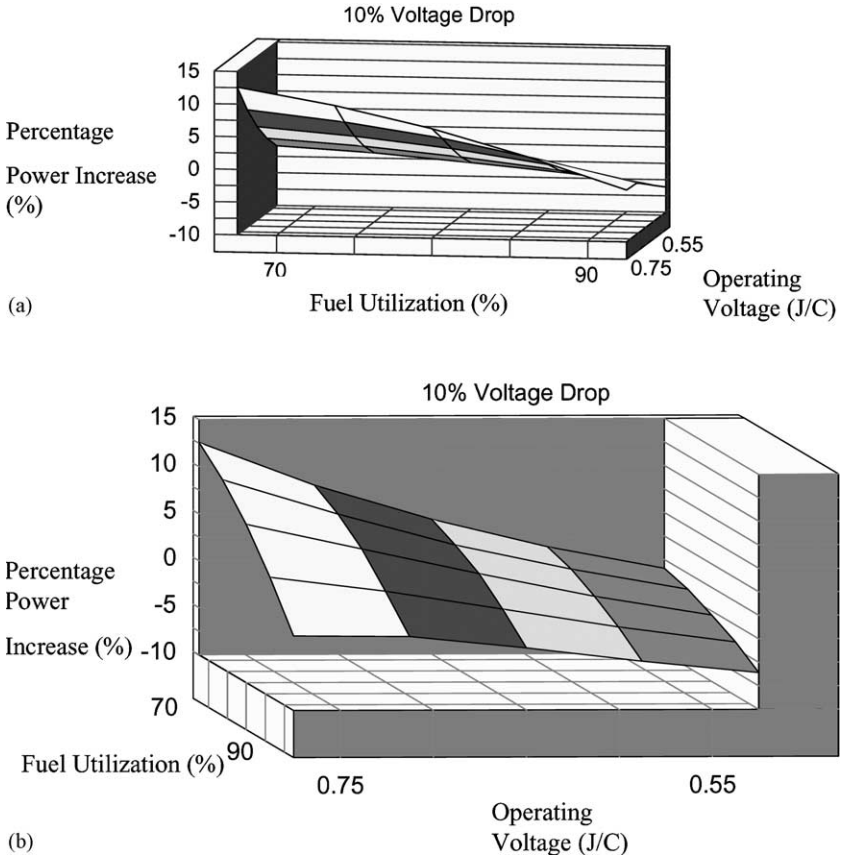

Fig. 12. (a) Net power increase as a function of fuel utilization; (b) Net power increase as a function of operating voltage.

reserve'' or ''fuel buffer'' present within the cell stack to help guard against reactant depletion [3]. Consider the following graph of power generation as a function of fuel utilization.

Again aside from varying fuel utilizations, the operating conditions are those of Table 1. In regions of large percentage fuel consumption, depletion issues such as concentration polarization hinder power generation. The second derivative of power generation is thus negative, indicating the increasing impact of reactant depletion at larger fuel utilizations. An increase in current that begins from an initially lower fuel utilization is then less prone to severe current and power dips.

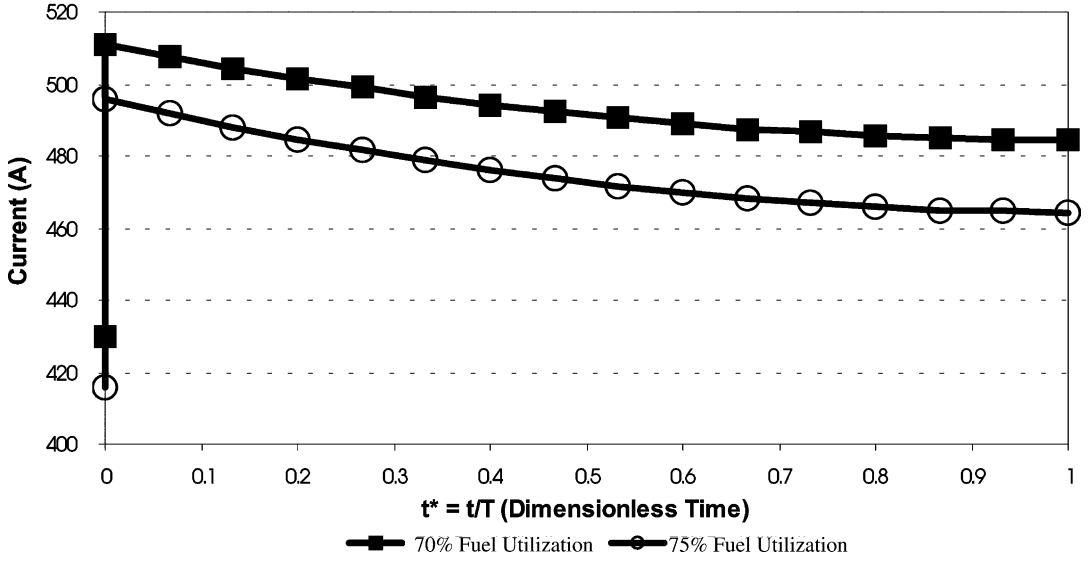

Fig. 13. Fuel utilizations' impact on current generation transients.

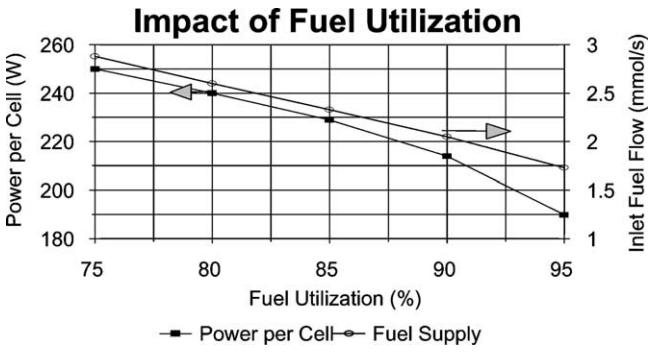

Fig. 14. Power and fuel supply variation vs. fuel utilization.

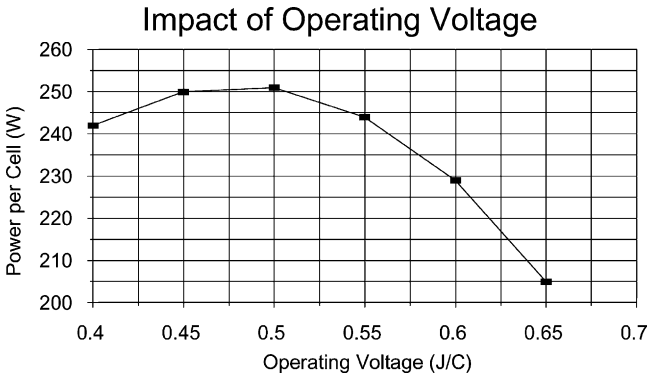

Fig. 15. Dependence of power generation upon operating voltage.

3.2. Larger initial operating voltages

Fig. 12 also shows that higher operating voltages better accommodate increases in cell stack load. Consider the dependence of power on voltage, as shown in the following figure.TSOFCs are nominally operated at 1000 °C and moderate fuel utilizations; these operating conditions diminish activation and concentration polarization. It is thus appropriate to present the following approximation:

$$P = iV_{\text{operate}} \tag{14}$$

$$P \cong \frac{(E - V_{\text{operate}})}{R_{\text{eff}}} V_{\text{operate}} \tag{15}$$

$$P \cong \frac{EV_{\text{operate}}}{R_{\text{eff}}} - \frac{V_{\text{operate}}^2}{R_{\text{eff}}} \tag{16}$$

Eq. (16) is a quadratic expression with voltage as the independent variable, hence the parabolic nature of Fig. 15. Continuing the development

$$\frac{\mathrm{d}P}{\mathrm{d}V_{\text{operate}}} \cong \frac{E - 2V_{\text{operate}}}{R_{\text{eff}}} \tag{17}$$

$$\frac{\mathrm{d}^2P}{\mathrm{d}V_{\text{operate}}^2} \cong \frac{-2}{R_{\text{eff}}} \tag{18}$$

The negative second derivative given in Eq. (18) explains the convex shape of the graph. Minh and Takahashi [21] presented a similar development. Physically, as operating voltage increases, there are the competing effects of *decreased* current generation with *rise* in voltage. At lower voltages, the latter effect is dominant and power increases. The power generation in this region, however, is unacceptably low. An extremum (i.e. maximum) is eventually reached, after which the decrease in current is more influential; thus, power decreases. A given voltage reduction increases power most dramatically, then, at higher operating voltages, because "*P–V*" slopes are steepest in this region. Higher operating voltages then not only allow for greater cell stack efficiencies but also facilitate *unslaved* increases in stack load.

3.3. Optimal reduction of cell potential

Reducing voltage increases current generation; however, as alluded to, current and voltage both contribute to cell power. Unslaved increases in stack power generation then require one to understand where the optima lie. As an example, consider a set of initial conditions wherein initial fuel utilization and operating voltage are 75% and 0.75 V, respectively. The lower fuel utilization and higher operating voltage are motivated by the findings reported within the

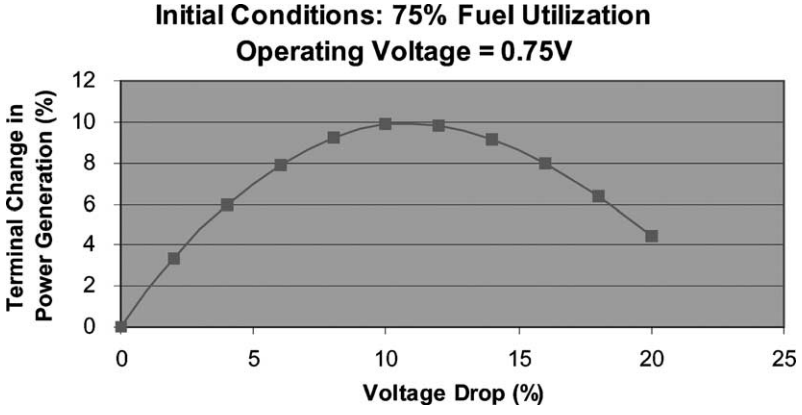

Fig. 16. Impact of percentage decrease in cell potential on percentage change-in-power generation.

previous sections. These changes in initial conditions, with respect to Table 1, are done with an understanding that a fuel utilization that is too low and an operating voltage that is too high may lead to poor fuel efficiency and power density, respectively.

Fig. 16 illustrates the impact operating voltage reductions have upon cell power generation.

In the given scenario, a maximum is reached when voltage is reduced approximately 11% (allowing a 10% increase in power generation). At this point, the increase in current is balanced by the decrease in operating voltage. Mapping such optima can facilitate fuel cell systems design wherein responses to moderate increases in load are done in a timely and robust manner. The requirement for such load-following enhancement is accurate dynamic simulation of the cell stack.

4. Conclusions

The response times of fuel cell systems to load-varying conditions may be diminished by allowing the cell stack to respond freely (i.e. *unslaved* to slower balance-of-plant components such as the fuel processor). A model has been produced for understanding the transient responses that result from unslaved load-following, with specific attention placed upon SiemensWestinghouse's TSOFC technology and increased load demand scenarios. As operating voltage decreases, current increases and thereby causes changes in reactant concentrations. These transient responses were modeled under the assumptions of quasi-steady-state electrochemistry and heat transfer. Additional simplifications were an invariant supply of reactants and lumped capacitance modeling. Finally, a Lagrangian approach was used to track fuel ''parcels'' throughout the electrical transients.

The initial spikes in current and power, after cell potential is lowered, are followed by *dips* in both. In the baseline, case study power actually decreased *below* its initial steady-state value. The increase in current diminishes reactant concentrations, thus increasing fuel utilization. The ensuing countereffect is a loss in current generation until a new electrical steady-state is reached. These dips highlight the need for accurate fuel cell dynamic simulation when attempting *unslaved* load-following. Fuel cell temperature increases due to greater current and inefficiency at lower operating voltages. Thermal response, however, is orders of magnitude slower than the electrical response; thus, the two phenomena may be considered as decoupled episodes.

Design efforts toward reliable, independent cell load-following should consider process parameters and their impact on cell response. Lowering the initial fuel utilization minimizes reactant depletion issues (i.e. concentration polarization, smaller Nernst potentials) and thus facilitates increased current. Larger initial cell potentials help accommodate greater load demand through the steep P–V slopes that occur at high voltages. Both of these trends may be incorporated within process design, so that the cell stack may more rapidly respond to demands for more power. Finally, the competing effects of current increase and voltage decrease result in optima, as far as percentage change-in-power generation versus decrease in cell potential.

A representative transient model of a mature fuel cell technology has been developed for cell stack dynamic simulation. The particular objective has been to identify the operating conditions that promote rapid increases in power generation. This has been done by decoupling the cell stack's response from that of balance-of-plant processes. In order for effective controls schemes to incorporate *unslaved* cell stack response, however, attention has to be returned to the additional subsystems. As an example, future microchannel fuel processors may be able to process changes in fuel demand in sub-second timescales; such an advance in fuel processing would require the ''invariant fuel supply'' assumption be reconsidered. Additionally, consider power conditioning. Changing cell potential to accommodate load change (in lieu of waiting for changes in reactants supply) must be amenable to system electronics. As an example, the user is referred to the synchronism requirement stated within the introduction. Future transient studies will include variations in fuel cell type (e.g. planar SOFCs), timely start-up dynamics (wherein thermal and electrochemical transport phenomena are coupled) and safe system shutdowns.

References

[1] A.J. Appleby, Characteristics of Fuel Cell Systems, in: L.J.M.J. Blomen, M.N. Mugerwa (Eds.), Fuel Cell Systems, Plenum Press, New York, 1993, pp. 179–181.
[2] K. Kordesch, G. Simader, Fuel Cells and Their Applications, VCH, Weinheim, 1996, pp. 13–14.
[3] T.G. Kreutz, J.M. Ogden, Transient Effects in Fuel Cell Vehicles with Onboard Fuel Processors, Fuel Cell Semin., 1998, pp. 663–665.
[4] E.A. Liese, R.S. Gemmen, F. Jabbari, J. Brouwer, Technical development issues and dynamic modeling of gas turbine and fuel cell hybrid systems, in: Proceedings of the 1999 International Gas Turbines Institute, Indianapolis, Indiana, 99-GT-360.
[5] J. Padulles, G.W. Ault, J.R. McDonald, An integrated SOFC plant dynamic model for power systems simulation, J. Power Sources 86 (2000) 495–500.
[6] T.Q. Minh, T. Takahashi, Science and Technology of Ceramic Fuel Cells, Elsevier, Amsterdam, 1995, p. 132.
[7] C.L. Haynes, W.J. Wepfer, Design for power of a commercial-grade tubular solid oxide fuel cell, Energy Conversion Manage. 41 (2000) 1123–1139. (Erratum 2063–2067).
[8] P. Costamagna, L. Magistri, A.F. Massardo, Design and part-load performance of a hybrid system based on a solid oxide fuel cell reactor and a micro-gas turbine, J. Power Sources 96 (2001) 352–368.
[9] E. Achenbach, Response of a solid oxide fuel cell to load change, J. Power Sources 57 (1995) 105–109.
[10] C.L. Haynes, W.J. Wepfer, Characterizing heat transfer within a commercial-grade tubular solid oxide fuel cell for enhanced

thermal management, Int. J. Hydrogen Energy 26 (4) (2001) 369–379.
[11] F.P. Incoprera, D.P. DeWitt, Fundamentals of Heat and Mass Transfer, 4th Edition, Wiley, New York, 1996, pp. 215–218.
[12] J.C. Amphlett, R.F. Mann, B.A. Peppley, P.R. Roberge, A. Rodrigues, A model predicting the transient responses of proton exchange membrane fuel cells, J. Power Sources 61 (1996) 183–188.
[13] S. Kakac, Y. Yener, Convective Heat Transfer, 2nd Edition, CRC Press, Boca Raton, 1995 (Chapter 8).
[14] R.S. Gemmen, E. Liese, J.G. Rivera, F. Jabbari, J. Brouwer, Development of Dynamic Modeling Tools for Solid Oxide and Molten Carbonate Hybrid Fuel Cell Gas Turbine Systems, in: Proceedings of the 2000 International Gas Turbines Institute, Munich, Germany, 2000.
[15] B.R. Munson, D.F. Young, T.H. Okiishi, Fundamentals of Fluid Mechanics, pp. 186–187.
[16] Y.S. Touloukian (Ed.), Thermophysical Properties of High Temperature Solid Materials, Vol. 4, Thermophysical Properties Research Center, Purdue University, 1967, pp. 3–48.
[17] C.L. Haynes, Simulation of Tubular Solid Oxide Fuel Cell Behavior for Integration into Gas Turbine Cycles, Ph.D. Dissertation, Georgia Institute of Technology, 1999.
[18] W.H. Press, B.P. Flannery, S.A. Teukolsky, W.T. Vetterling, Numerical Recipes: The Art of Scientific Computing, Cambridge University Press, Cambridge, 1986, p. 574.
[19] R.A. George, N.F. Bessette, Reducing the manufacturing cost of tubular SOFC technology, J. Power Sources 71 (1998) 131–137.
[20] J.H. Hirschenhofer, D.B. Stauffer, R.R. Engelman, Fuel Cells: A Handbook (Rev. 3), US DOE Office of Fossil Energy, Morgantown, 1994.
[21] T.Q. Minh, T. Takahashi, Science and Technology of Ceramic Fuel Cells, Elsevier, Amsterdam, 1995, pp. 25–27.